Science Press

ARTICLE

EMI Shielding Performance and Mechanical Properties of Proton Acid Treated $Ti_3C_2T_x$ *MX*ene/CNT Composite

Liu Xingmin,   Yang Jihua,   Lu Shaowei,   Yang Dongxu,   Wang Jijie,   Liu Chunzhong, Wang Sai

College of Materials Science and Engineering, Shenyang Aerospace University, Shenyang 110136, China

Abstract: After the colloidal proton acid treatment, the preparation of titanium carbide $Ti_3C_2T_x$ was achieved. In addition, the single-walled carbon nanotube (SWCNT) was used as reinforcement to improve the mechanical properties of proton acid treated titanium carbide (H-*MX*ene): the tensile property is enhanced by nearly 400% while the electromagnetic shielding performance is retained. This study demonstrates that the H-*MX*ene and carbon nanotube have great potential in electromagnetic interference (EMI) shielding composite materials with excellent mechanical properties.

Key words: titanium carbide; *MX*ene; SWCNT; EMI shielding

The proliferation of new generation electronic device leads to the increasing electromagnetic (EM) radiation pollution. Exposure to electromagnetic interference (EMI) can cause negative effects in various fields, including the medicine, military, and navigation[1–2]. Therefore, EMI shielding materials are crucial. The primary function of EMI shielding material is to reflect radiation by charge carriers which directly interact with EM fields[3]. Metals (Cu, Ag) are commonly used as EMI shielding material[4], but they are heavy and stiff, which seriously restricts their application in EMI shielding field[5]. New generation EMI material should be light, flexible, and more geometrically malleable.

Recently, a 2D transition metal with carbide and/or nitride, namely *MX*ene ($M_{n+1}X_n$ene, $n=1-3$; *M* stands for transition metal; *X* is carbon and/or nitrogen; ene stands for graphene), gradually becomes one of the most applicable EMI composite materials. Besides, *MXT* ($M_{n+1}X_nT_x$, $n=1-3$; *T* represents a terminating group) material[6] is further developed based on *MX*ene material.

$Ti_3C_2T_x$ material possesses extraordinary electrical conductivity[7] and is commonly used in sensors[8–9], energy stor-

age[10–11], and EMI shielding[12–13]. According to the EM wave shielding theory, the magnitude of the induced current directly affects the shielding effect[14], thereby enhancing the electrical properties of materials. However, the surface of 2D $Ti_3C_2T_x$ material is covered by Ti(II)/Ti(III)-suboxide, -hydroxide, or -fluoride, which can be easily oxidized into Ti(IV)-oxide. In addition, the H_2O/O_2 diffusion in the bulk material can also accelerate the oxidation degradation of $Ti_3C_2T_x$ material[15]. With the spread of the intercalant during the exfoliation process, the interaction of $Ti_3C_2T_x$ material is weakened, therefore severely restricting the application of $Ti_3C_2T_x$ material.

Proton acid treatment can remove the intercalant, such as Li^+, dimethylsulfoxide, and tetraalkylammonium hydroxide[16]. Thereby, the reinforcement of hydration stability can be achieved. The proton acid of 6 mol/L H^+ was used as the trigger to desorb the intercalant from the nanosheet surface. By gradually adding protic acid into the matrix solution, the suspension of closely aligned $Ti_3C_2T_x$ stacks was prepared. Then the products were identified as H-$Ti_3C_2T_x$ film. Compared with that of the specimens without acid treatment, the conductivity of $Ti_3C_2T_x$ films is greatly increased from 3×

10^5 S/m to 4.5×10^5 S/m.

Although the proton acid treatment improves the electrical property of $Ti_3C_2T_x$ material, its mechanical property and flexibility still need enhancement. According to Ref. [17−18], the tensile strength and flexibility of *MX*ene films prepared by vacuum filtration are unsatisfied. Therefore, the single-walled carbon nanotubes (SWCNTs) with superb mechanical properties were used as reinforcement in this research because of their seamless defect-free cylindrical graphitic structure. According to Ref. [19−20], it is confirmed that SWCNT is an effective reinforcement. Through the combination of carbon nanotubes and $Ti_3C_2T_x$ material, $Ti_3C_2T_x$/SWCNT composite materials with different ratios were prepared in this research. The enhancement in mechanical property is achieved, and an EM shielding effectiveness which is comparable to that of the pure H-$Ti_3C_2T_x$ materials can also be retained, presenting further development of two-dimensional EM shielding material.

1 Experiment

Ti_3AlC_2 (0.038 μm, AR, 99%, Ningbo Jinlei Nano Material Technology Co., Ltd), high-purity SWCNT powder (95%, Chengdu Organic Chemicals Co., Ltd), lithium fluoride (LiF, AR, 99%, Shanghai Macklin Biochemical Co., Ltd), hydrochloric acid (9 mol/L, Tianjin Fengchuan Chemical Reagent Co., Ltd) were used in this research.

Vacuum-assisted filtration (180 W, water-circulation multifunction vacuum pump, Shanghai Jinfu Experimental Equipment Co., Ltd), cellulose separator membrane (pore size of 0.22 μm, Shanghai Xinya Purification Equipment Co., Ltd), scanning electron microscope (SEM, Zeiss Gemini SEM500/300), and X-ray diffractometer (XRD, DX-2700BH, Haoyuan Instrument Co., Ltd) were used in this research. Tensile tests were conducted with the Instron material testing system (XM-DZSC001).

*MX*ene of $Ti_3C_2T_x$ material was prepared by selective etching of the Ti_3AlC_2 precursor, as shown in Fig. 1 (Step I). The etching solution was prepared by slowly adding 1.6 g lithium fluoride into 20 mL hydrochloric acid solution (9 mol/L) with stirring for about 5 min. Then, 1 g Ti_3AlC_2 powder was added into the solution intermittently. Via ice bath, the reaction temperature was strictly controlled below 10 ° C to avoid oxidation. After the powder addition, the mixture was stirred at room temperature for 24 h. The deionized water was used to wash the acid mixture via centrifugation at 3500 r/min for several times (5 min for each cycle) until pH≈6. Then the solution was ultrasonically cleaned for 20 min for the delamination of multi-layer *MX*ene. High-purity argon gas circulation treatment was used to prevent oxidation. Finally, the solution was freeze-dried to calibrate the content of delaminated *MX*ene (Step II in Fig.1).

During vigorous stirring, 6 mol/L HCl was added dropwise into the delaminated *MX*ene suspension until pH=1 for the proton acid treatment. Then obvious coagulation in the solution could be observed. The solution was placed in centrifuge at 5000 r/min, and the upper liquid was abandoned

(Step III and Step IV). Repeat this process for several times until pH=6 and the proton acid-treated *MX*ene, namely H-*MX*ene material, was prepared. The degree of solute coagulation in the solution was gradually decreased with increasing the pH value.

SWCNT powder (0.5 g) was put into a grinder. Extract 2 mL triton solution, inject it into the SWCNT powder uniformly, and then grind them clockwise for 40 min. The deionized water was used to wash the grinder and the grinding rod, and the used water was separately collected in the large beakers. The used water was stirred for 2.5 h with stirring head in the middle position of the used water. Then the solution was ultrasonically cleaned with the ultrasonic probe inserted into the solution. The ultrasonic wave was released every 1 s and last for 1 s. The whole process lasted for 60 min.

SWCNT of different contents was added into *MX*ene and H-*MX*ene materials to prepare SWCNT/*MX*ene and SWCNT/H⁺-introduced *MX*ene mixtures, respectively. After SWCNT addition, the mixture was subjected to magnetic stirring at 300 r/min for 1 h for uniform mixture. Then, the specimen films were prepared by vacuum-assisted filtration (Step V and Step VI). The mass ratio of SWCNT to *MX*ene was 3:1, 5:1, 10:1, 15:1, and 20:1, and the corresponding specimen was named as SCM3, SCM5, SCM10, SCM15, amd SCM20, respectively. Similarly, the ratio of SWCNT to H-*MX*ene was 3:1, 5:1, 10:1, 15:1, and 20:1, and the corresponding specimen was named as SCHM3, SCHM5, SCHM10, SCHM15, amd SCHM20, respectively.

2 Results and Discussion

2.1 Characterization

Significant *MX*ene coagulation can be observed in the solution during the proton acid treatment with low pH values. This phenomenon is attributed to the charge screening effect of cations[21]: the proton acid shifts the zeta potential of $Ti_3C_2T_x$ nanosheets to a relatively positive one, destabilizing $Ti_3C_2T_x$ colloids. Chen et al[22] analyzed the reduced activity of protons in titration experiments and concluded that the coagulation of *MX*ene layers in the early stages of proton acid treatment is mainly caused by the formation of hydrogen bonds between layers and the hydrophobic action of reaction layer surface.

According to Ref. [23], the intercalated Li⁺ ions lead to the stabilization of intercalated H_2O in multi-layered $Ti_3C_2T_x$ material. XRD patterns of *MX*ene and H-*MX*ene materials are shown in Fig. 2. It is revealed that H-*MX*ene material has a clearly smaller interlayer distance than *MX*ene material does. The strong and sharp peak of (002) plane can be detected in both two materials, proving the good alignment of *MX*ene nanosheets. With the proton acid treatment proceeding, the *d*-spacing is decreased from 1.592 43 nm (*MX*ene) to 1.400 04 nm (H-*MX*ene). These phenomena all result from the decrease in intercalated H_2O between $Ti_3C_2T_x$ layers.

The surface of proton acid-treated $Ti_3C_2T_x$ material, i. e., H-*MX*ene material, shows more undulation and folds than the *MX*ene material does, implying that the self-assembly of
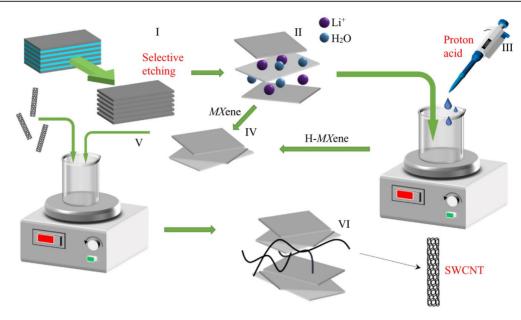
Fig.1   Schematic diagrams of preparation process of SWCNT/MXene and SWCNT/H-MXene materials
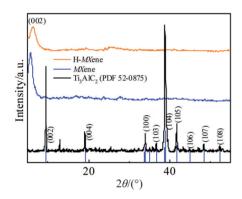

Fig.2   XRD patterns of MXene and H-MXene materials

$Ti_3C_2T_x$ nanosheets during proton acid process results in the formation of larger aggregates. According to Fig. 3, the dominant laminar structure can be clearly observed in all specimens. In addition, the layer spacing reduction is obvious in H-MXene material, compared with that of the MXene material. The film thickness of H-MXene material is also thinner than that of MXene material after vacuum-assisted filtration. The H^+ introduction declines the disorder in stacking and reunion process of MXene flakes (Fig. 3a and 3b). According to Fig. 3c and 3d, SWCNT is densely distributed between the MXene layers in the SCM20 and SCHM20 specimens, indicating the formation of 1D/2D hybrid network.

2.2 Performance

All SWCNT/MXene and SWCNT/H-MXene specimens were prepared via vacuum-assisted filtration and vacuum-dried at 60 °C for 2 h. The initial concentration of MXene material in suspension is 2.24 mg/mL and it changes to 1.05 mg/mL after introduction of 0.1 mol/L H^+. The coagulation of MXene layers exists the whole time during the washing stage. The average thickness of the SWCNT/H-MXene film is 10

μm. With increasing the SWCNT content in the composite, the color of specimen is changed from gray black to dark black, as shown in Fig. 4. Besides, the surface of specimen after proton acid treatment is flawless and flat (Fig.4b).

EMI shielding performance tests of X-band (8.20 – 12.4 GHz) were conducted for SWCNT/MXene and SWCNT/H-MXene materials with different ratios via vector network analyzer (PAN-L N5230C Agilent Technologies, waveguide). The specimens were sliced into a rectangular form of 22.9 mm×10.2 mm. The scattering parameters (S_{11}, S_{12}, and S_{21}) of all specimens were recorded. The reflection (R), transmission (T), absorption (A), reflection shielding effectiveness (SE_R), absorption shielding effectiveness (SE_A), and total EMI shielding effectiveness (SE_T) can be calculated by Eq. (1 – 6), respectively:

$$R=|S_{11}|^2=|S_{12}|^2 \tag{1}$$

$$T=|S_{12}|^2=|S_{21}|^2 \tag{2}$$

$$R+A+T=1 \tag{3}$$

$$SE_R = 10\lg\left(\frac{1}{1-R}\right) = 10\lg\left(\frac{1}{1-|S_{11}|^2}\right) \tag{4}$$

$$SE_A = 10\lg\left(\frac{1-R}{T}\right)10\lg\left(\frac{1-|S_{11}|^2}{|S_{21}|^2}\right) \tag{5}$$

$$SE_T=SE_A+SE_R+SE_M \tag{6}$$

where SE_M represents the multiple internal reflection of material (usually negligible when $SE_T \geqslant 15$ dB[24]). The total EMI shielding effectiveness (SE_T) of different materials is shown in Fig.5.

According to EM theory, with increasing the frequency, the EM radiation capacity is increased, and EM harassment tends to the far field area, resulting in the non-negligible negative effects on electric and magnetic fields[24]. Because the electric and magnetic fields of high-frequency EM waves characterized by radiation are interdependent, shielding one of
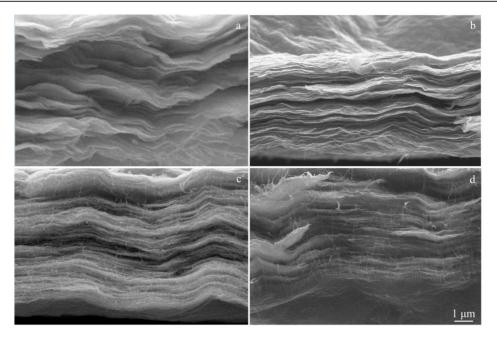
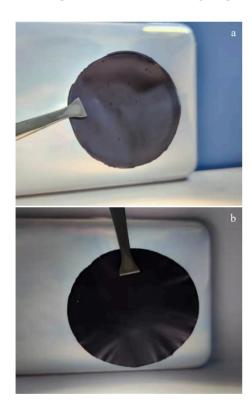Fig.3   SEM cross-sectional morphologies of *MX*ene (a), H-*MX*ene (b), SCM20 (c), and SCHM20 (d) materials

Fig.4   Appearances of *MX*ene (a) and SCHM5 (b) materials

Fig.5   Total EMI shielding effectiveness of different materials

them is enough to achieve superb effects in practice. Based on Schelkunoff formula[24] and Simon principle[25], shielding effectiveness (SE) is proportional to the relative conductivity of shielding materials, which is consistent with the high conductivity of H-*MX*ene material (4000−5000 S/cm). The specific shielding effectiveness (*SSE*) can be used to evaluate the EM shielding performance of materials. However, it only considers the material density (*d*), which is not sufficient.
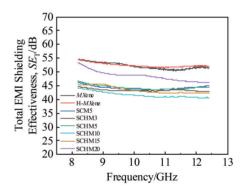
Therefore, the absolute shielding effectiveness (dB·cm^2·g^{-1}), which simultaneously considers the density *d* and thickness *t* of material, is introduced, as follows:

$$SSE/t = SE/tb \tag{7}$$

The absolute shielding effectiveness can directly reflect the material performance, which is calculated based on the normalization of SE_T with respect to density and thickness. High *SSE*/*t* values are crucial for the lightweight shielding materials. Fig.6 and Fig.7 show the SE performance, absolute shielding effectiveness, and EC of different materials. It can be seen that the absolute shielding effectiveness of H-*MX*ene material is several times higher than that of the *MX*ene material. The proton acid treatment reduces the spacing between *MX*ene layers, leading to a better conductivity of H-*MX*ene material. Besides, the introduction of SWCNTs barely causes a negative effect on EMI shielding performance of *MX*ene material. Table 1 shows the comparison of EMI shielding performance of different materials. Due to the abundant free electrons on the surface of *MX*ene and SWCNT/ H-*MX*ene materials[35], the *MX*ene flake can directly reflect
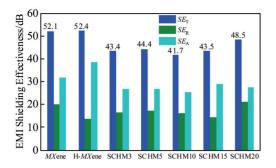
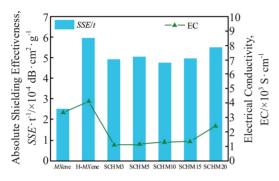Fig.6　EMI shielding effectiveness (X-band) of different materials

Fig.7　Absolute shielding effectiveness (SSE/t) and electrical conductivity (EC) of different materials

some EM waves when they come into connect. Because of the well-aligned layered structure of *MX*ene materials (Fig.3a and 3b) and the ohm loss caused by the high electron density, the energy of the remaining EM waves declines when they pass through the flakes. As EM waves are transmitted to a new *MX*ene layer, the process is repeated (Fig. 8). The multiple internal reflection loss inside the shield material is negligible once the total shielding effectiveness is more than 15 dB. However, this conclusion does not apply to the *MX*ene material with the multi-layered structure. According to Fig.6, SE_A accounts for more than 50% of the total shielding

effectiveness of all materials. Actually, SE_M is included in SE_A because the EM waves are absorbed or dissipated in the form of heat within the material[36]. In addition, the dipoles can be produced on the surface of *MX*ene flakes between the termination group and titanium, which improves the overall shielding performance by interacting with EM waves. The EMI absolute shielding effectiveness of SWCNT is 127.9 dB·cm²·g⁻¹, which is much lower than that of the prepared *MX*ene material. Because SWCNT is at nanoscale, it is suitable to enhance the mechanical properties and environmental adaptability of the matrix without influence on the base EM shielding performance. The introduction of SWCNT results in smoother surface and greater flexibility of H-*MX*ene materials: SCHM3 film can bend of nearly 180° and the film surface only has minor folding scratches after recovery. According to Ref. [37 – 39], the tensile strength of carbon nanotubes is nearly three times higher than that of the *MX*ene material. Thus, the introduction of SWCNT can greatly improve the tensile strength of *MX*ene material.

The film specimens for stretch performance tests were prepared by vacuum-assisted filtration with the thickness of 8– 10 μm, gauge length of 5 mm, and width of 3 mm. Stress and strain were recorded at extension rate of 1 mm·min⁻¹. More than three strips of each type of specimens were tested via XM-DZSC001 equipment (Yitong Testing Equipment Technology Co., Ltd) with load cell of 10 N. The fracture surface is perpendicular to the loading direction. According to Ref.[38], the ultrasonic pretreatment for 30 min can compact the layered MXene materials, i. e., the $Ti_3C_2T_x$ flakes are stacked more tightly. According to Fig.3a and 3b, the spacing between $Ti_3C_2T_x$ flakes reduces, which leads to the increase in tensile strength of *MX*ene material (Fig. 9). With the introduction of SWCNT, the tensile strength of *MX*ene material is further enhanced. The tensile strength of SCHM3 specimen is 128.8 MPa, which is almost 6 and 4 times higher than that of the *MX*ene and H-*MX*ene materials. The cross-sectional morphologies of the failed strips (Fig. 3) indicate that $Ti_3C_2T_x$ material has a flat, straight, and brittle-like fracture surface, which is a common fracture

Table 1　EMI shielding performance of different materials

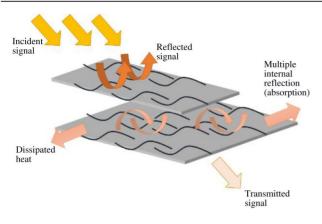| Type	Material	Absolute shielding effectiveness/dB·cm²·g⁻¹	Ref.
Metal-based	Copper	32.3	[26]
	Al foil	30 555	[27]
	CuNi-carbon nanotubes	1 580	[28]
	Cu foil	7 812	[27]
	Ag nanowire	2 416	[29]
Carbon-based	Carbon foam	1 250	[30]
	Reduced graphene oxide (rGO)	692	[31]
	rGO/Fe₃O₄	1 033	[32]
	SWCNT/epoxy	72	[33]
*MX*ene-based	$Ti_3C_2T_x$/carbon nanofibers	2 647	[34]
	$Ti_3C_2T_x$-sodium alginate	30 830	[27]
	$Ti_3C_2T_x$-SWCNT	49 336–55 204	-

Fig.8 EMI shielding mechanism of *MX*ene layer structure

morphology of 2D film materials[40–41]. Because the $Ti_3C_2T_x$ film is stacked as lamellar structure, the applied tensile stress is maintained by the shear stress transfer between overlapping $Ti_3C_2T_x$ flakes and by the straining of the flakes. The overlapping causes the relative slipping between the flakes, and then a critical transverse crack at the junction of adjacent flakes is formed and propagated rapidly, resulting in

strip failure.

The tensile-fracture process of *MX*ene material can be divided into three stages: straightening, linear elasticity, and plastic deformation[38]. After proton acid treatment, *MX*ene material exhibits a state of nearly complete linear elastic-plastic deformation tension. This phenomenon reveals that the introduction of H^+ greatly shortens the straightening process. Since the proton acid treatment also decreases the sheet spacing in *MX*ene material, the straightening process is basically completed during the extraction process. With the SWCNT introduction of different contents, the stretching patterns gradually recover. It can be observed that SWCNT distributed between layers reduces the fracture formation and increases the tensile strength and toughness of materials. The EMI shielding ability and tensile strength of SCHM3 specimen are comparable to those of other EMI shielding materials, as shown in Table 2. SCHM3 specimen has the absolute shielding effectiveness of 49 336 $dB·cm^2·g^{-1}$, which is comparable to that of the *MX*ene material. A great increase in tensile strength (128.8 MPa) is also achieved for SCHM3 specimen. Therefore, compared with those of *MX*ene materials, the absolute shielding effectiveness and the tensile
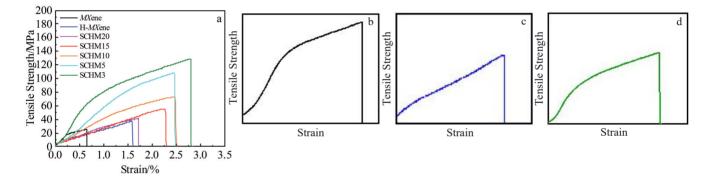

Fig.9 Tensile strength of different materials (a); schematic diagrams of tensile strength curve of *MX*ene (b), H-*MX*ene (c) and SCHM3 (d) materials

Table 2 Absolute shielding effectiveness and tensile strength of different materials

Material	Absolute shielding effectiveness/$dB·cm^2·g^{-1}$	Tensile strength/MPa	Ref.
Copper	32.26	366.00	[27]
PEI/graphene	166.54	5.50	[42]
Carbon fiber/PC film	1 201.74	115.10	[43]
FSPF film	1 2607.4	0.94	[44]
CEF-NF	6 294.02	20.74	[45]
NCF	30 039.42	11.21	[46]
MWCNT-NCF composite	23 223.86	68.28	[46]
Stainless steel	27.46	515.00	[27]
PI-rGO foam	937.46	11.40	[47]
SCHM3	49 336	128.80	-

Note: PEI-poly(ethylene imine); PC-polycarbonate; FSPF-Fe_3O_4@SiO_2@polypyrrole; CEF-carbon fiber or polypropylene/polyethylene core/sheath bicomponent fiber; NF-nonwoven fabric; MWCNT-multiwalled carbon nanotube; NCF-neat carbon fabric; PI-polyimide

strength are increased by 200% and 400% for the SCHM3 specimen, respectively.

3 Conclusions

1) Singe-walled carbon nanotube (SWCNT) as the reinforcement can effectively improve the tensile properties of transition metal with carbide and/or nitride (*MX*ene) materials with slight influence on the absolute electromagnetic shielding performance.

2) *MX*ene material after proton acid treatment (H-*MX*ene) with the SWCNT addition (mass ratio of H-*MX*ene to SWCNT is 3∶1) has the absolute shielding effectiveness of 49 336 dB·cm^2·g^{-1} and the tensile strength of 128.8 MPa, which are increased by 200% and 400%, respectively, compared with those of *MX*ene materials.

3) The *MX*ene materials show great potential in electromagnetic shielding composites, which should be further developed.

References

1 Chandra R B J, Shivamurthy B, Kulkarni S D *et al. Mater Res Express*[J], 2019, 6(8): 82 008

2 Tan D C, Jiang C M, Li Q K *et al. J Mater Sci Mater Electron*[J], 2021, 32(21): 25 603

3 Chung D D L. *Carbon*[J], 2001, 39(2): 279

4 Voronin A S, Fadeev Y V, Govorun I V *et al. Journal of Materials Science*[J], 2021, 56(26): 14 741

5 Geetha S, Satheesh K K K, Rao C R K *et al. J Appl Polym Sci*[J], 2009, 112(4): 2073

6 Naguib M, Kurtoglu M, Presser V *et al. Adv Mater*[J], 2011, 23(37): 4248

7 Shayesteh Z A, Mirkhani S A, Sun P C *et al. Nanoscale*[J], 2021, 13(6): 3572

8 Li T K, Chen L L, Yang X *et al. J Mater Chem C*[J], 2019, 7(4): 1022

9 Kim S J, Koh H J, Ren C E *et al. ACS Nano*[J], 2018, 12(2): 986

10 Naguib M, Come J, Dyatkin B *et al. Electrochem Commun*[J], 2012, 16(1): 61

11 Yang Q, Huang Z D, Li X L *et al. ACS Nano*[J], 2019, 13(7): 8275

12 Yun T, Kim H, Iqbal A *et al. Adv Mater*[J], 2020, 32(9): 1 906 769

13 Li X L, Yin X W, Liang S *et al. Carbon*[J], 2019, 146: 210

14 Gargama H, Chaturvedi S K, Thakur A K. *J Electromagn Waves Appl*[J], 2014, 28(6): 765

15 Iqbal A, Hong J, Ko T Y *et al. Nano Converg*[J], 2021, 8(1): 1

16 Berdiyorov G R. *Europhysics Letters*[J], 2015, 111(6): 67 002

17 An H, Habib T, Shah S *et al. Sci Adv*[J], 2018, 4(3): eaaq0118

18 Ling Z, Ren C E, Zhao M Q *et al. Proc Natl Acad Sci*[J], 2014, 111(47): 16 676

19 Zhang B, Luo C, Zhou G M *et al. Adv Funct Mater*[J], 2021, 31(26): 2 100 793

20 Barshutina M N, Volkov V S, Arsenin A V *et al. Materials*[J], 2021, 14(9): 2418

21 Natu V, Sokol M, Verger L *et al. J Phys Chem C*[J], 2018, 122(48): 27 745

22 Chen H W, Wen Y Y, Qi Y Y *et al. Adv Funct Mater*[J], 2020, 30(5): 1 906 996

23 Ghidiu M, Halim J, Kota S *et al. Chem Mater*[J], 2016, 28(10): 3507

24 Liu Shunhua, Liu Junmin, Dong Xinglong *et al. Electromagnetic Shielding and Absorbing Materials*[M]. Beijing: Chemical Industry Press, 2014 (in Chinese)

25 Simon R M. *Polym-Plast Technol Eng*[J], 1981, 17(1): 1

26 Shui X P, Chung D D L. *J Electron Mater*[J], 1997, 26(8): 928

27 Shahzad F, Alhabeb M, Hatter C B *et al. Science*[J], 2016, 353(6304): 1137

28 Ji K J, Zhao H H, Zhang J *et al. Appl Surf Sci*[J], 2014, 311: 351

29 Ma J J, Wang K, Zhan M. *RSC Adv*[J], 2015, 5(80): 65 283

30 Moglie F, Micheli D, Laurenzi S *et al. Carbon*[J], 2012, 50(5): 1972

31 Yan D X, Pang H, Li B *et al. Adv Funct Mater*[J], 2015, 25(4): 559

32 Song W L, Guan X T, Fan L Z *et al. J Mater Chem A*[J], 2015, 3(5): 2097

33 Huang Y, Li N, Ma Y F *et al. Carbon*[J], 2007, 45(8): 1614

34 Cao W T, Chen F F, Zhu Y J *et al. ACS Nano*[J], 2018, 12(5): 4583

35 Zhang H B, Yan Q, Zheng W G *et al. ACS Appl Mater Interfaces*[J], 2011, 3(3): 918

36 Ameli A, Nofar M, Wang S *et al. ACS Appl Mater Interfaces*[J], 2014, 6(14): 11 091

37 Zhang M S, Li M, Wang S K *et al. Mater Des*[J], 2017, 117: 37

38 Luo S H, Patole S, Anwer S *et al. Nanotechnology*[J], 2020, 31(39): 395 704

39 Li F, Cheng H M, Bai S *et al. Appl Phys Lett*[J], 2000, 77(20): 3161

40 Li Y Q, Yu T, Yang T Y *et al. Adv Mater*[J], 2012, 24(25): 3426

41 Chen H, Müller M B, Gilmore K J *et al. Adv Mater*[J], 2008, 20(18): 3557

42 Ling J Q, Zhai W T, Feng W W *et al. ACS Appl Mater Interfaces*[J], 2013, 5(7): 2677

43 Tang W J, Lu L S, Xing D *et al. Compos Part B Eng*[J], 2018, 152: 8

44 Yuan Y, Yin W L, Yang M L *et al. Carbon*[J], 2018, 130: 59

45 Lu L S, Xing D, Teh K S *et al. Mater Des*[J], 2017, 120: 354

46 Pothupitiya G S S J, Yang K H, Braveenth R *et al. Materials*[J], 2017, 10(12): 1350

47 Li Y, Pei X, Shen B *et al. RSC Adv*[J], 2015, 5(31): 24 342

质子酸处理二维碳化钛/碳纳米管复合材料的电磁屏蔽性能与机械性能

刘兴民，杨吉华，卢少微，杨东旭，王继杰，刘春忠，王　赛

(沈阳航空航天大学 材料科学与工程学院，辽宁 沈阳 110136)

摘　要： 通过质子酸胶体处理，实现了碳化钛 $Ti_3C_2T_x$ 的制备。此外，使用单壁碳纳米管（SWCNT）作为增强成分，提升了质子酸处理碳化钛（H-*MX*ene）的机械性能——不仅保持了电磁屏蔽性能，而且将拉伸性能提升了近400%。结果表明，H-*MX*ene 和碳纳米管具有作为高机械性能电磁（EMI）屏蔽复合材料的潜力。

关键词： 钛化碳；*MX*ene；SWCNT；EMI屏蔽